
Article:
Zhu, Z., Provis, J.L. and Chen, H. (2018) Quantification of the influences of aggregate shape and sampling method on the overestimation of ITZ thickness in cementitious materials. Powder Technology, 326. pp. 168-180. ISSN: 0032-5910

https://doi.org/10.1016/j.powtec.2017.12.008

This is a preprint of a paper published in Powder Technology. The version of record can be found at https://doi.org/10.1016/j.powtec.2017.12.008

Quantification of the influences of aggregate shape and sampling method on the overestimation of ITZ thickness in cementitious materials

Zhigang Zhu [a], John L. Provis [b], Huisu Chen [a,*]

[a] Jiangsu Key Laboratory of Construction Materials, School of Materials Science and Engineering, Southeast University, Nanjing 211189, China

[b] Department of Materials Science and Engineering, University of Sheffield, Sheffield S1 3JD, United Kingdom

* Corresponding author. Tel.: +86 25 52090645; Fax: +86 25 52090667

E-mail: chenhs@seu.edu.cn

Abstract

The microstructure of the interfacial transition zone (ITZ) surrounding the aggregate in a cementitious composite is quite different from that of the bulk matrix, because of its distinct physical nature including relatively high porosity and low rigidity. The thickness and volume fraction of the ITZ play a major role in determining the transport and mechanical behaviour of cementitious composites. However, the ITZ thickness may be overestimated when undertaking sectional plane analysis of these composites. Analysis of Platonic particles has previously shown that the sphericity of the particle is an important parameter in determining the overestimation of the ITZ thickness, but this raises the question of whether sphericity is sufficient to uniquely characterize the influence of aggregate shape. This paper investigates the influence of particle shape on overestimation of ITZ thickness for aggregate shapes which have the same sphericity values as Platonic particles; specifically, spheroids of differing geometries. A normal line sampling algorithm, which is designed to replicate the practical experimental process used in ITZ determination, is employed to obtain the apparent ITZ thickness. The influences of particle shape, sampling method and particle size distribution are investigated in terms of the overestimation of the ITZ volume fraction, and the effective diffusivity within three-phase composites, using the differential effective medium approximation.

Keywords: ITZ thickness, spheroidal particle, Platonic particles, sphericity, diffusivity.

1. Introduction

The interfacial transition zone (ITZ) surrounding the aggregate particles is an important phase within a cementitious composite structure [1, 2]. This is because the ITZ is more porous than bulk cement paste. The formation and evolution of the ITZ are affected by many factors, including: wall effects which effectively repel solid grains from a solid surface, flocculation of cement grains, micro-bleeding giving a locally higher water/cement ratio, nucleation and precipitation of specific phases such as portlandite, one-sided growth, and gel syneresis [3, 4]. Thus, the ITZ is considered to be a ‘weak link’ when describing or predicting the macroscopic

This is a preprint of a paper published in Powder Technology. The version of record can be found at https://doi.org/10.1016/j.powtec.2017.12.008

performance of cementitious composites, such as mechanical and transport properties [5-16]. To better understand the influence of the ITZ microstructure on the macroscopic performance of the composite as a whole [17], it is necessary to quantify the thickness and volume fraction of the ITZ [18-20]. However, the actual ITZ thickness (here denoted t) is difficult to measure because the constituents of most composites are opaque. Normally, a backscattered electron (BSE) image of a polished cross-section through a concrete sample is used to obtain information about the microscopic morphology of concrete [21-24]. Then, successive strips based on a concentric expansion method near the aggregate are employed to examine the ITZ microstructure, as shown in Fig. 1(a). However, since an arbitrary cross-section rarely passes through the normal of the aggregate surface, such an approach yields an apparent ITZ thickness t' which is larger than the actual ITZ thickness t, as shown in Fig. 1(b).

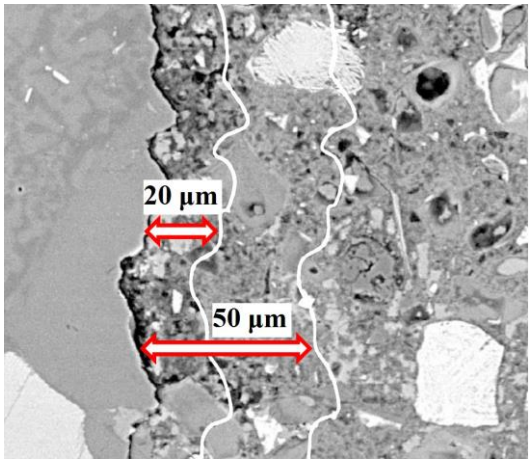

(a) Backscattered electron image of concrete [25]

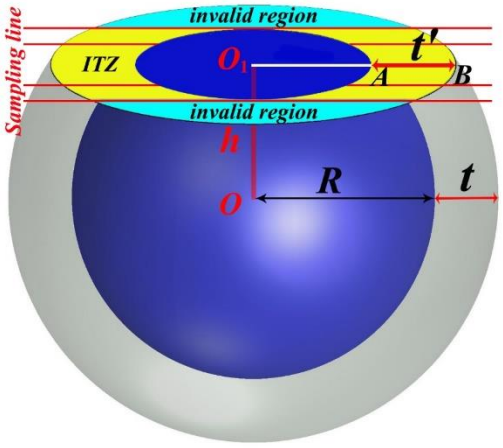

(b) Schematic of the apparent ITZ thickness t' and the actual ITZ thickness t for a spherical aggregate, ($t' > t$)

Fig. 1. Measurement of ITZ thickness around aggregate in numerical simulation and image analysis

Many researchers have worked to survey the degree of overestimation between the apparent and the actual ITZ thickness. Stroeven [26] proposed a formula to quantify the degree of overestimation of ITZ thickness around a circular aggregate particle. Chen et al. [27] derived analytical solutions for two-dimensional (2D) rectangular and elliptical aggregates, and Zhu and Chen [28] investigated the overestimation of ITZ thickness around regular polygonal and elliptical aggregate particles under the same circularity conditions. Chen et al. [29] developed a generalized analytical formula for the overestimation of the ITZ thickness around convex-shaped grains, as given in Eq.(1).

$$t' = 2\left(1-k_{invalid}\right)\left(t+\frac{2\pi B}{S}t^2+\frac{4\pi}{3S}t^3\right) \underset{\text{then } k_{invalid}\to 0}{\overset{\text{if } t<<S}{\approx}} 2t \tag{1}$$

where B and S respectively represent the mean Feret (caliper) diameter and the surface area of a particle. It is evident that only when a sampling plane crosses through the aggregate, can the analysis of ITZ thickness start to be conducted in practice, as shown in Fig. 1(a). In other words, if the section plane crosses the ITZ region but not the aggregate, it is not possible to be certain from a 2D section whether this porous paste region in fact belongs to the ITZ layer. So, such a region of uncertainty is called an *invalid region*. The ratio of the volume of the invalid region to the total volume of the ITZ region, as shown in Fig. 1(b), is then defined as the invalid coefficient $k_{invalid}$ which appears in Eq.(1).

This is a preprint of a paper published in Powder Technology. The version of record can be found at https://doi.org/10.1016/j.powtec.2017.12.008

The invalid coefficient $k_{invalid}$ corresponding to spherical particles has been studied [29]. However, it is much more difficult to determine the invalid coefficient for non-spherical particles. Recently, based on a process which is similar to the Minkowski sum in mathematical morphology [30, 31], Chen et al. [32] proposed a methodology to accurately construct the ITZ layers surrounding Platonic particles (i.e., tetrahedron, cube, octahedron, dodecahedron, icosahedron [33]). They further extended the calculation of the invalid coefficient from spheres to Platonic particles by using a systematic line sampling (SLS) algorithm, including both sampling planes and sampling lines. Taking an arbitrary sampling plane in Fig. 2(a) as an example, the normal of the sampling plane is determined based on its spatial orientation, defined by angles (θ_i,ϕ_j), then the spacing ΔL_{3D} between two adjacent sampling planes is used to control the density of the sampling planes. For a specified sampling plane, the sampling lines traversing the entire sampling plane in all orientations are defined by the scanning planar angle step $\Delta\alpha$, and the spacing ΔL_{2D} between two adjacent parallel sampling lines is used to control the density of the sampling lines.

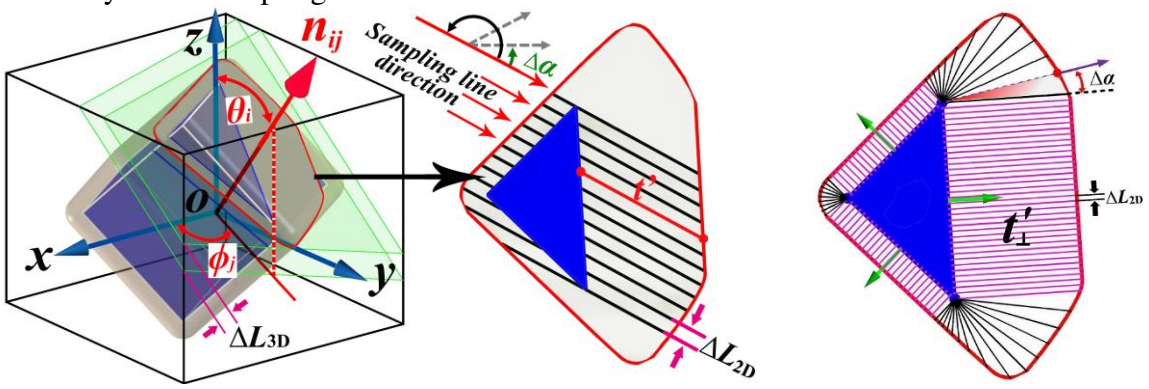

(a) SLS algorithm [32] (b) NLS algorithm [34]

Fig. 2. Two sampling methods for Platonic particles

Moreover, Fig. 2(a) shows that a series of parallel sampling lines are oriented in all potential directions in a given sampling plane, rather than only in the direction normal to the aggregate boundary. In conventional quantitative image analysis experiment as shown in Fig. 1(a), the profiles of strip delineation are always arranged parallel to the outer boundary of the aggregate in the given section plane, although the section plane itself could be of any orientation. The thickness of the ITZ layer can then be determined based on the distribution curve of a specified phase, or of porosity in cases where this rather than a difference in mineralogical phases is the defining characteristic of the ITZ [35], as a function of the distance along the normal of the aggregate boundary. So, the statistical average of the apparent ITZ thickness via the SLS algorithm is not consistent with the conventional experimental results, obtained e.g. by BSE image analysis, because the sampling line in the SLS algorithm is not perpendicular to the aggregate boundary. Therefore, Zhu et al. [34] further proposed a normal line sampling (NLS) algorithm (details can be seen in Section 3.1) to accurately evaluate the ITZ thickness along the normal of a Platonic aggregate boundary, as shown in Fig. 2(b).

So far, the studies on the statistical relationship of apparent to actual ITZ thickness have only focused on Platonic and spherical aggregate particles; it is necessary to extend this study to other non-spherical particles, and even to concave particles, to represent actual aggregates such as those which have been reconstructed by a spherical harmonic function approach [36-38] in Fig. 3(a). According to the visualization of the ITZ layer around a concave polygon as shown

This is a preprint of a paper published in Powder Technology. The version of record can be found at https://doi.org/10.1016/j.powtec.2017.12.008

in Fig. 3(b), the outer profile of the ITZ layer around concave particle is even more complex than that around a convex particle in Fig. 3(c). Therefore, we still restrict our study here to the convex particle system.

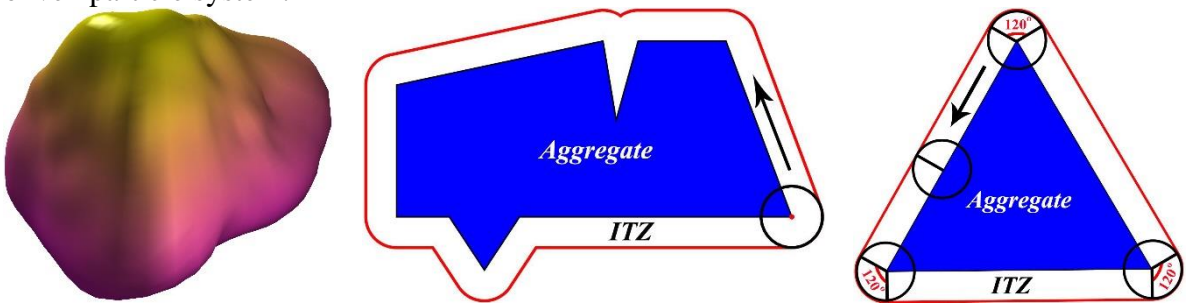

(a) A star-shaped particle (b) ITZ layer around a concave polygon (c) ITZ layer around a convex polygon (regular triangle [28])

Fig. 3. Schematic of a concave particle (star-shaped) and the ITZ layer around arbitrary polygons

It was determined in our previous study for Platonic particles [32, 34] that the sphericity of the particle, which is a shape descriptor for the particle itself, is important in determining the value of t'/t at a given ratio of actual ITZ thickness to equivalent particle diameter t/D_{eq} (where D_{eq} is the diameter of a sphere with the same volume as a given particle). Specifically, the results showed that the values of t'/t decrease with increasing sphericity for both sampling methods. This raises the question of whether sphericity is a sufficient and unique parameter which can characterize the influence of aggregate shape on t'/t at a given value of t/D_{eq}. Spheroidal particles offer the easiest example to investigate this, because the sphericities of both oblate and prolate ellipsoids can be specified to be exactly equal to that of a particular Platonic particle by adjusting their aspect ratios. In addition, we can obtain a spheroid with arbitrary sphericity by changing aspect ratios, and spheroids can represent a wide range of shapes from very platy to elongated [39], which is more flexible than Platonic particles. Recently, Zhu and Chen [40] also employed the SLS algorithm to obtain $k_{invalid}$ for spheroidal particles, and examined the influence of particle shape on the overestimation of the ITZ thickness around spheroidal particles which have the same sphericity as Platonic particles.

Therefore, this paper intends to investigate the influence of the particle shape for spheroidal and Platonic particles with matching sphericity, and to evaluate the differences between the two sampling methods (NLS and SLS) for spheroidal particles. For this purpose, the NLS algorithm, which is much closer to the practical experimental process, is adopted for spheroidal particles to obtain the apparent ITZ thickness. Furthermore, for polydisperse packed particles, the influences of particle shape, particle size distribution (PSD) and sampling method on the degree of overestimation of the statistical average of the ITZ thickness, ITZ volume fraction and effective diffusivity (based on differential effective medium approximation) within the composite are investigated.

2. ITZ layer around ellipsoidal particles

The equation of a tri-axial ellipsoid (denoted as E) centered at the origin with semi-axes a, b and c aligned along the coordinate axes, is expressed in Eq.(2).

$$E: \quad \frac{x^2}{a^2}+\frac{y^2}{b^2}+\frac{z^2}{c^2}=1 \tag{2}$$

This is a preprint of a paper published in Powder Technology. The version of record can be found at https://doi.org/10.1016/j.powtec.2017.12.008

An ellipsoid of revolution (spheroid) has a pair of equal semi-axes (a=b) and a distinct third semi-axis (c) which is an axis of symmetry. The ellipsoid is prolate or oblate when c is respectively greater than or smaller than a. The aspect ratio of a spheroid, usually denoted κ, is defined as $\kappa = c/a$. The relationship between κ and equivalent spherical diameter D_{eq} of the spheroid is given in Eq.(3).

$$D_{eq} = 2c\kappa^{-2/3} = 2a\kappa^{1/3} \tag{3}$$

Because a real ITZ will have significant heterogeneity when defined and measured experimentally, the structure of the ITZ is not strictly a uniform shell of constant thickness. However, at present, it is very difficult to study ITZ layers with non-uniform thickness. So, for the purposes of this work, we assume that the ITZ layer is a uniform shell of constant thickness around an aggregate particle. In our previous study, we have proposed a methodology to construct an ITZ layer with uniform thickness around an ellipsoid [40]. The construction process is determined by a vector of constant length drawn from any point of the particle surface in the direction of the surface exterior normal, which is similar to the Minkowski sum in mathematical morphology [30, 31]. This study mainly considers the ITZ layer around oblate and prolate ellipsoids which have the same sphericities as the five different Platonic particles [32]. The sphericity (s; $0 < s \leq 1$) of a particle is defined as the ratio of the surface area of a sphere to that of a given particle with the same volume [32, 41]. The aspect ratios of these spheroidal particles with semi-axes $a : b : c = 1 : 1 : \kappa$ are given in Table 1. The volume of a tri-axial ellipsoid is V=4πabc/3, and the corresponding surface area S is given in Eq.(4) [42].

$$S = \begin{cases} 2\pi a^2 + \pi(c^2/\varepsilon) ln\dfrac{1+\varepsilon}{1-\varepsilon}, & \text{Oblate } (c < a) \\ 2\pi a^2 + 2\pi(c^2/\varepsilon)\arcsin(a\varepsilon/c), & \text{Prolate } (c > a) \end{cases} \tag{4}$$

where $\varepsilon = \sqrt{|1-(c/a)^2|}$.

Table 1 Geometry of spheroidal particles with the same sphericity values as the Platonic particles

Polyhedron	Sphericity, s	Oblate ellipsoid (a:b:c)	Prolate ellipsoid (a:b:c)
Tetrahedron	0.671	1 : 1 : 0.229	1 : 1 : 6.625
Cube (Hexahedron)	0.806	1 : 1 : 0.344	1 : 1 : 3.593
Octahedron	0.846	1 : 1 : 0.391	1 : 1 : 3.007
Dodecahedron	0.910	1 : 1 : 0.495	1 : 1 : 2.204
Icosahedron	0.939	1 : 1 : 0.562	1 : 1 : 1.884

3. Sectional plane analysis

Sectional plane analysis has commonly been used to study ITZ microstructure because image analysis techniques applied to 2D sections provide a method to obtain structural information for composites. Similarly, a sectional plane analysis algorithm [36] is employed in computer simulations to obtain the morphology of the ellipsoidal particle surrounded by an ITZ layer. Actually, the cross-section of a spheroidal particle can be either a circle (for sampling planes parallel to an equator, i.e., perpendicular to the symmetry axis) or an ellipse (otherwise). The elliptical cross-section can be characterized by its minor and major principal semi-axes [43]

This is a preprint of a paper published in Powder Technology. The version of record can be found at https://doi.org/10.1016/j.powtec.2017.12.008

which are denoted as m and M, respectively, as shown in Fig. 4. The equation of the elliptical cross-section is given in Eq.(5).

$$\begin{cases} m = \sqrt{a^2 - \dfrac{(1-e_0^2)p^2}{1-e_0^2\sin^2\theta}}, & \text{Prolate } (c > a) \\ M = \sqrt{a^2 - \dfrac{p^2}{1-e_0^2\cos^2\theta}}, & \text{Oblate } (c < a) \end{cases} \tag{5}$$

where p is the distance from the center of the spheroid to the cross-section measured normal to the cross-section plane, and $\theta \in [0, \pi/2]$ is the angle between the symmetry axis of the spheroid and the normal of the sampling plane. The eccentricity e_0 of the spheroid is described by its minor and major semi-axes, as given in Eq.(6).

$$e_0^2 = \begin{cases} 1-a^2/c^2, & \text{Prolate } (c > a) \\ 1-c^2/a^2, & \text{Oblate } (c < a) \end{cases} \tag{6}$$

The eccentricity e ($0 \le e < 1$) of the elliptical cross-section is defined by $e^2 = 1 - m^2/M^2$. The relationship between e and e_0 is given in Eq.(7).

$$e^2 = \begin{cases} e_0^2\sin^2\theta, & \text{Prolate } (c > a) \\ \dfrac{e_0^2\sin^2\theta}{1-e_0^2\cos^2\theta}, & \text{Oblate } (c < a) \end{cases} \tag{7}$$

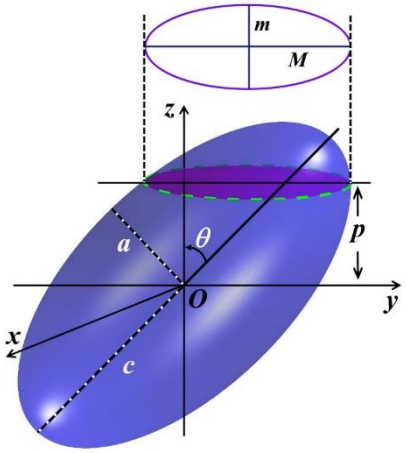

Fig. 4. Schematic of the elliptical cross-section for a prolate ellipsoid

In this section, for a given sampling plane, the apparent ITZ thickness along the normal line at the aggregate boundary will be described in detail. Then, the line sampling rule of the NLS algorithm is established for spheroidal particles, and applied to obtain the apparent ITZ thickness around a single particle.

3.1. NLS algorithm

Having obtained the morphologies of the ITZ and aggregate on a cross-section for a spheroidal particle, a method similar to the practical image analysis technique as shown in Fig. 1(a) is needed to measure the apparent ITZ thickness. Therefore, the normal line sampling (NLS) algorithm previously presented for Platonic particles [34] is adopted. Since the ITZ region exists in the vicinity of the aggregate, only those sampling planes crossing through both the aggregate

and ITZ regions are considered. In three-dimensional (3D) space, an arbitrary sampling plane can be defined by two components, i.e., a normal vector and a point location. As shown in Fig. 5(a), a normal vector n_{ij} of the $(i, j)^{th}$ sampling plane is given by ($\sin(\theta_i)\cos(\phi_j)$, $\sin(\theta_i)\sin(\phi_j)$, $\cos(\theta_i)$) based on its spatial angle (θ_i,ϕ_j), where $0 \le \theta_i,\phi_j \le \pi$, for $1 \le i \le N_\theta$ and $1 \le j \le N_\phi$. Here, N_θ is the total number of uniformly divided polar angle increments measured from the zenith direction (z-axis), and N_ϕ is the total number of uniformly divided azimuthal angle increments measured from the azimuth reference direction (x-axis) to the orthogonal projection of the normal vector on the reference plane xoy. For the sake of simplification, we specify $N_\theta = N_\phi$ in this paper. The point location is used to fix the position of the sampling plane in 3D space, and is chosen as a division point of a projected segment [36] of the aggregate particle onto the normal of the sampling plane. Fig. 5(b) shows a schematic view of a projected segment PQ of an ellipsoidal particle onto the normal vector n_{ij}, and the projected segment is divided into $|PQ|/\Delta L_{3D}$ (rounded to the nearest integer) increments based on the spacing ΔL_{3D} between two adjacent sampling planes.

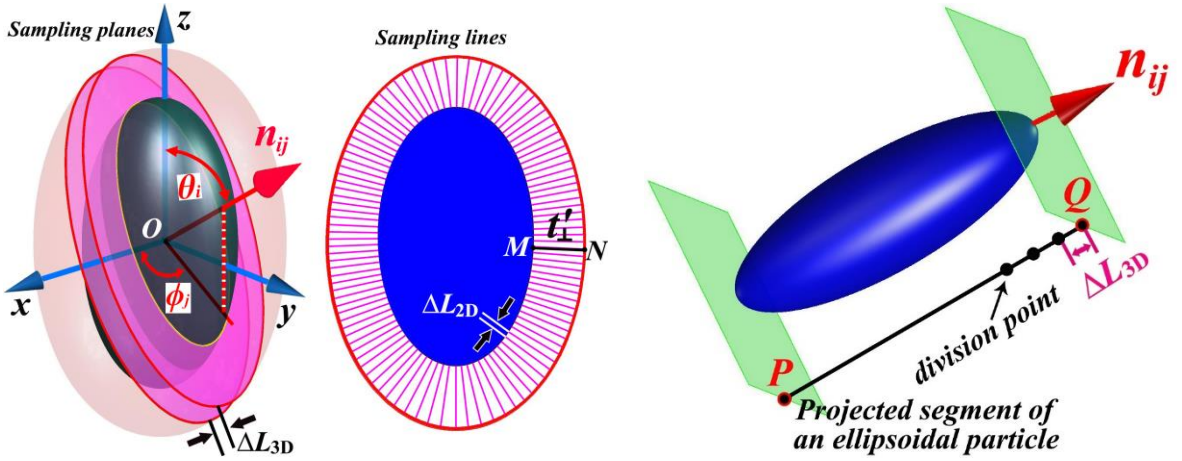

(a) Sampling planes and sampling lines in the NLS algorithm

(b) Projected segment PQ of an ellipsoidal particle on the normal vector n_{ij} [40]

Fig. 5. Schematic of the normal line sampling algorithm for an ellipsoidal particle

For a given sampling plane crossing through the spheroidal aggregate, as shown in Fig. 5(a), we can find the boundaries of the aggregate particle and its corresponding ITZ layer, respectively. The apparent ITZ thickness along the exterior normal vector of the boundary of the aggregate can be obtained using the NLS algorithm. To ensure that the sampling lines are uniformly distributed, a set of sampling lines which are perpendicular to the boundary of the aggregate, and the spacing ΔL_{2D} between two adjacent sampling lines, need to be determined. To this end, ΔL_{2D} is defined specifically as the distance between the intersection points of two adjacent sampling lines with the boundary of the aggregate. In this study, for the sake of simplification, we set $\Delta L_{2D} = \Delta L_{3D}$. A sampling line perpendicular to the boundary of the aggregate and intersecting with the boundary of the ITZ layer returns a line segment MN as shown in Fig. 5(a). The length of the line segment MN is the apparent ITZ thickness, i.e., $t_\perp' = |MN|$.

This is a preprint of a paper published in Powder Technology. The version of record can be found at https://doi.org/10.1016/j.powtec.2017.12.008

From this description of the NLS algorithm, the statistical average apparent ITZ thickness for a spherical particle (as a special case of the more general relationships for spheroids) can be analytically derived, Eq.(8).

$$\begin{aligned} t_{\perp}' &= \int_0^R \left(\sqrt{(R+t)^2 - h^2} - \sqrt{R^2 - h^2} \right) * \frac{1}{R} dh \\ &= \frac{1}{2} \sqrt{\left(1+\frac{t}{R}\right)^2 - 1} + \frac{1}{2}\left(1+\frac{t}{R}\right)^2 \arcsin\left(\frac{1}{1+t/R}\right) - \frac{\pi}{4} \end{aligned} \tag{8}$$

where R is the radius of the spherical particle, and h is the height from the center of the sphere to the sampling plane, as shown in Fig. 1(b).

Taking an ellipsoidal particle with ITZ thickness t as an example, as shown in Fig. 6, a sampling line which is parallel to the minor principal axis and crosses through the center of the ellipsoid is used to verify the reliability of the NLS algorithm. The numerical values of the apparent ITZ thickness are: $|AB| = 1.0000t$ and $|CD| = 1.0000t$. Theoretically, the lengths of AB and CD should be equal to t. This indicates that the numerical values are consistent with their corresponding theoretical values. Therefore, the NLS algorithm is reliable and accurate.

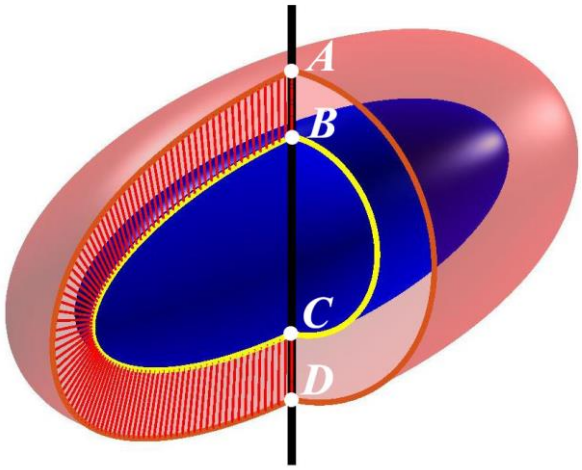

Fig. 6. Verification of the ITZ thickness for a specified sampling line

3.2. Line sampling rule of the NLS algorithm for spheroidal particles

The key issue to guarantee a reliable statistical analysis of the apparent ITZ thickness is to determine how many sampling lines are appropriate for spheroidal particles. According to the above description of the algorithm, four parameters may affect the result of the apparent ITZ thickness: N_θ, N_ϕ, ΔL_{3D} and ΔL_{2D}. Based on the specification, as described above, of $N_\theta = N_\phi$ and $\Delta L_{3D} = \Delta L_{2D}$, the strategy to determine the line sampling rule becomes to observe when the curves of $t_{\perp}'/t$ become stable with respect to an increase in the number of sampling lines. In other words, we need to address: (a) determination of the spacing ΔL_{3D} when N_θ is specified, and (b) determination of the value of N_θ when the spacing ΔL_{3D} is fixed.

Firstly, using $t/D_{eq} = 0.01$ and $N_\theta = N_\phi = 10$, the influence of $\Delta L_{3D}/D_{eq}$ on the ratio of the apparent to the actual ITZ thickness $t_{\perp}'/t$ is investigated. Fig. 7(a) shows that the curves of

$t_\perp'/t$ become stable with decreasing $\Delta L_{3D}/D_{eq}$; when $\Delta L_{3D}/D_{eq}$ is less than 0.005, there is no further change in $t_\perp'/t$. So, the spacing $\Delta L_{3D} = \Delta L_{2D} = 0.005 D_{eq}$ is selected as the line sampling rule for the NLS algorithm to give an accurate value of $t_\perp'/t$.

Secondly, we need to determine how many spatial angle increments are needed for spheroidal particles under the given conditions: t/D_{eq} = 0.01 and $\Delta L_{3D} = \Delta L_{2D} = 0.005 D_{eq}$. It can be seen from Fig. 7(b) that the values of $t_\perp'/t$ for oblate ellipsoids increase with an increase in N_θ, while $t_\perp'/t$ for prolate ellipsoids decreases with increasing N_θ. The curves of $t_\perp'/t$ become stable when $N_\theta \geq 20$, so that accurate values of $t_\perp'/t$ can be obtained when $N_\theta = N_\phi = 20$.

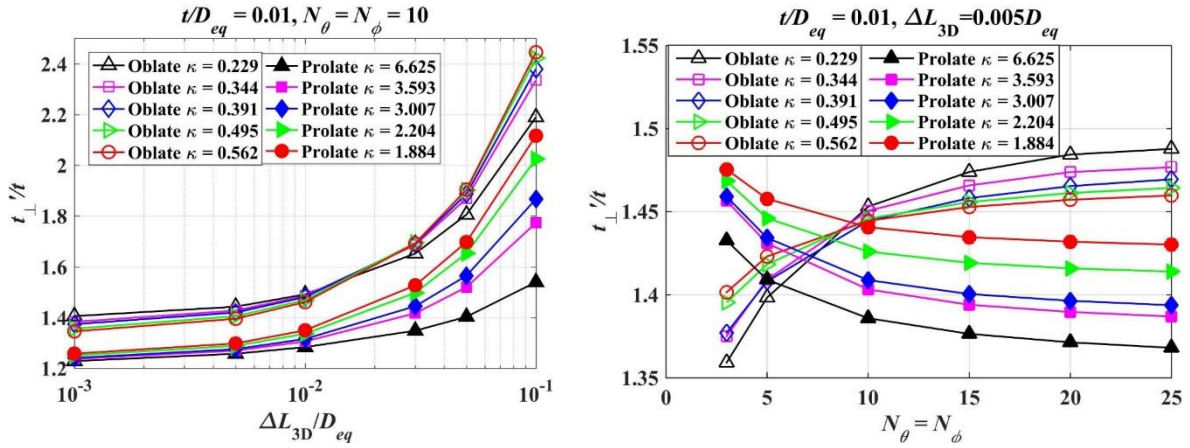

(a) The spacing ΔL_{3D} (b) The number of spatial directions N_θ (= N_ϕ)

Fig. 7. Determination of the spacing ΔL_{3D} and the number of spatial directions N_θ

Consequently, the line sampling rule of the NLS algorithm $N_\theta = N_\phi = 20$, $\Delta L_{3D} = \Delta L_{2D} = 0.005 D_{eq}$ may be adopted. To further confirm the reliability of this rule, the influence of the total number of sampling lines on both probability density curves and cumulative probability curves of $t_\perp'/t$ is considered in Appendix A.

3.3. Application of the NLS algorithm to a single spheroidal particle

Based on the line sampling rule described above, the influence on the overestimation of the ITZ thickness of the ratio of the actual ITZ thickness to the particle size t/D_{eq} will be considered in this section. To achieve this, we analyze three types of particle shapes with the same sphericity (Platonic; oblate and prolate ellipsoids) and two sampling methods (SLS [40] and NLS). Fig. 8(a) indicates that increasing t/D_{eq} results in a lower value of $t_\perp'/t$ for both oblate and prolate ellipsoids. In addition, $t_\perp'/t$ in Fig. 8(a) decreases with increasing sphericity for oblate ellipsoidal particles, but increases for prolate ellipsoidal particles. Compared with the spherical particle (sphericity s = 1), the ranking of the degree of overestimation of the ITZ thickness is: oblate ellipsoid > sphere > prolate ellipsoid. Most importantly, the curves of $t_\perp'/t$ tend toward the curve of $t_\perp'/t$ for a spherical particle (s = 1), Eq.(8), for both oblate and prolate ellipsoids with increasing sphericity. However, for the same sphericity, the three kinds

This is a preprint of a paper published in Powder Technology. The version of record can be found at https://doi.org/10.1016/j.powtec.2017.12.008

of particle shapes (i.e. oblate ellipsoid, prolate ellipsoid and Platonic particle) have different impacts on $t_\perp'/t$, as shown in Fig. 8(b-f). Thus, the sphericity of a particle is an important parameter to quantitatively characterize the effect of particle shape on the values of $t_\perp'/t$, but it is not a unique one, nor is it sufficient to define this relationship. The degree of overestimation of $t_\perp'/t$ is greater for oblate ellipsoids than for prolate ellipsoids, although the gap between oblate and prolate ellipsoids decreases with increasing sphericity. No clear trend exists between Platonic and spheroidal particles under the same sphericity conditions.

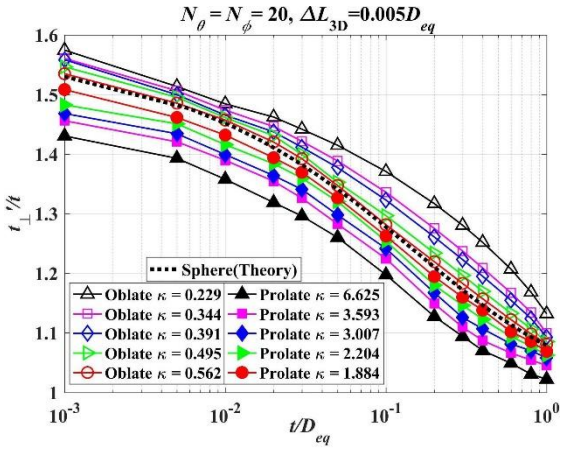

(a) Spheroidal and spherical particles (note logarithmic horizontal coordinate)

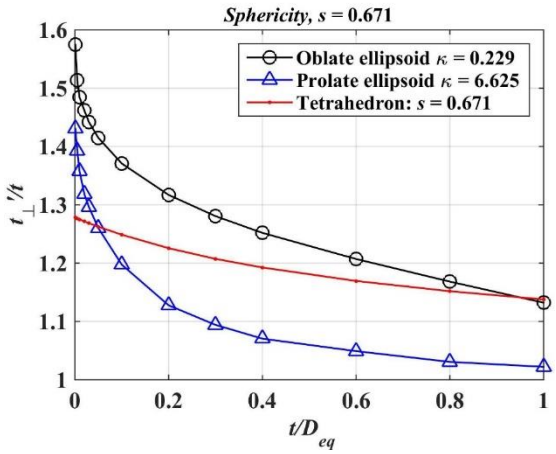

(b) Sphericity, s = 0.671

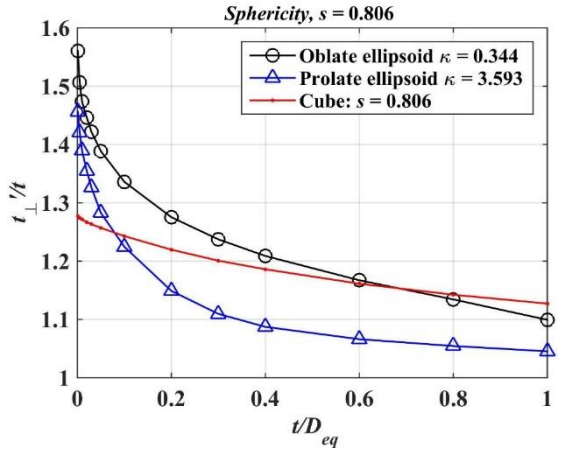

(c) Sphericity, s = 0.806

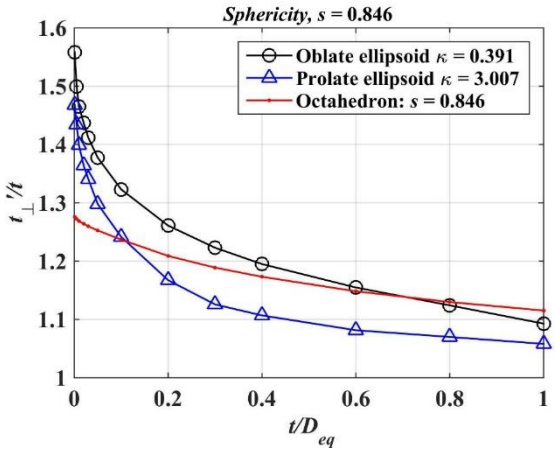

(d) Sphericity, s = 0.846

This is a preprint of a paper published in Powder Technology. The version of record can be found at https://doi.org/10.1016/j.powtec.2017.12.008

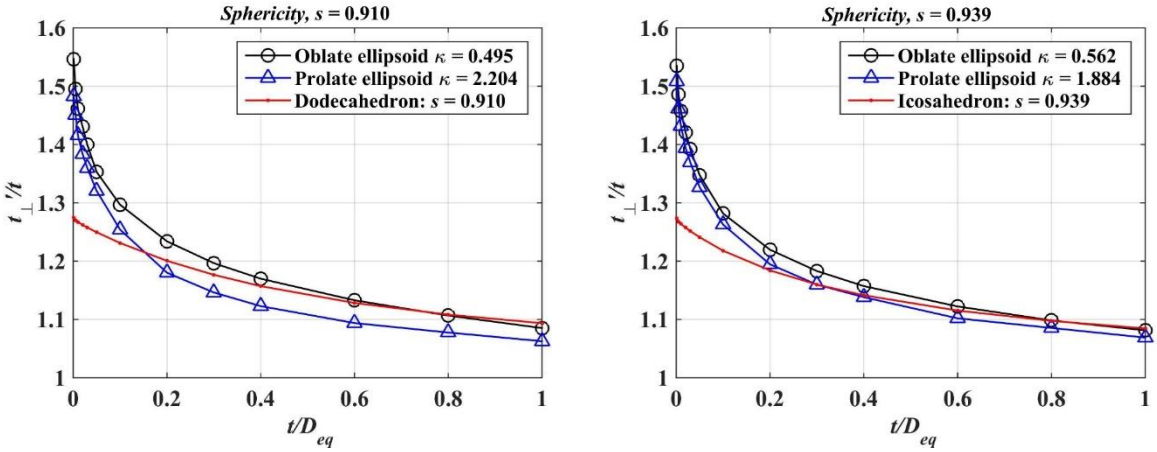

(e) Sphericity, s = 0.910 (f) Sphericity, s = 0.939

Fig. 8. Effect of particle shape on the overestimation of the ITZ thickness

Results obtained using the SLS algorithm [40] for spheroidal particles were also collected to analyze the differences between the two sampling methods. Fig. 9 shows that the degree of overestimation of the ITZ thickness in the NLS algorithm is less than that in the SLS algorithm for both oblate and prolate ellipsoids.

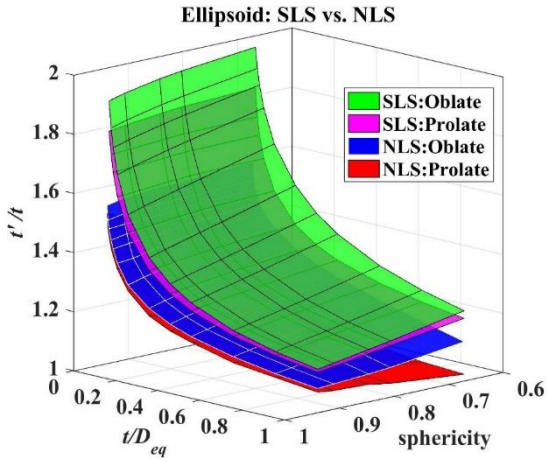

Fig. 9. Effect of sampling method for spheroidal particles on the overestimation of the ITZ thickness

Researchers may also be interested to calculate the difference between the influence of spheroidal and spherical particles on the degree of overestimation of the ITZ thickness; this is discussed in Appendix B.

4. Influence of particle size distribution on overestimation of the ITZ thickness

To extend these results to real concretes, assemblages of aggregate particles with various sizes must be investigated, as the aggregate in concrete is a polydisperse particle packing system. Thus, we must determine the effect of particle size distribution on a statistical average apparent ITZ thickness. The Fuller distribution function, Eq.(9), is commonly used to characterize the aggregate size distribution in concrete, and is used here as the basis of the discussion, but the

methodology presented in this paper may also be extended to other PSD functions such as the equivalent volume function [44, 45] or discrete sieve curves. It is noted that inter-particle interactions (including potential intersections between neighbouring ITZ regions) are excluded from this analysis.

$$F_V(D_{eq}) = \frac{\sqrt{D_{eq}} - \sqrt{D_{eq\_min}}}{\sqrt{D_{eq\_max}} - \sqrt{D_{eq\_min}}} \tag{9}$$

where $F_V(D_{eq})$ is the volume-based cumulative probability function; and D_{eq_min} and D_{eq_max} respectively represent the minimum and maximum equivalent spherical diameter of particles.

The number-based probability density function $f_N(D_{eq})$ given in Eq.(10) can be derived from Eq.(9) to generate the number of aggregate particles with different sizes [32].

$$f_N(D_{eq}) = \frac{5}{2D_{eq}^{7/2}(D_{eq\_min}^{-5/2} - D_{eq\_max}^{-5/2})} \tag{10}$$

The statistical average of the apparent ITZ thickness $t_N^{\perp\prime}$ for a polydisperse aggregate system with a Fuller distribution thus can be expressed as:

$$t_N^{\perp\prime} = \int_{D_{eq\_min}}^{D_{eq\_max}} t_\perp' f_N(D_{eq}) dD_{eq} \tag{11}$$

It is clear from Eq.(11) that the degree of overestimation of $t_N^{\perp\prime}$ is affected by the aggregate particle shape and PSD, and we also want to know the influence of sampling method on the ratio of $t_N^{\perp\prime}/t$. Firstly, the effect of particle shape on $t_N^{\perp\prime}/t$ is examined in Fig. 10(a) for a given PSD following the Fuller 0.25-10 mm distribution (D_{eq_min} = 0.25 mm and D_{eq_max} = 10 mm). Normally, the actual ITZ thickness is in the range 20 – 50 μm [25]. It can be seen from Fig. 10(a) that the curves of $t_N^{\perp\prime}/t$ decrease with increasing actual ITZ thickness. The values of $t_N^{\perp\prime}/t$ at the same actual ITZ thickness decrease with increasing sphericity for oblate ellipsoidal particles, but increase for prolate ellipsoidal particles. Compared with the spherical particle (sphericity s = 1), the degree of overestimation of the statistical average ITZ thickness is consistent with the single-particle case: oblate ellipsoid > sphere > prolate ellipsoid. The asymptotic line is still the curve of $t_N^{\perp\prime}/t$ for spherical particles. However, under the same sphericity conditions, the values of $t_N^{\perp\prime}/t$ for oblate ellipsoids are larger than for prolate ellipsoids.

Secondly, taking three types of particle shapes with the same sphericity s = 0.671 as an example, i.e., oblate κ = 0.229, prolate κ = 6.625 and the tetrahedron, Fig. 10(b) shows that the order of the degree of overestimation of $t_N^{\perp\prime}/t$ is: oblate ellipsoid > tetrahedron > prolate ellipsoid.

Thirdly, when we consider the difference between two sampling methods, Fig. 10(c) shows that the degree of overestimation of the statistical average ITZ thickness in the NLS algorithm is less than that in the SLS algorithm for both oblate and prolate ellipsoids.

Lastly, the influence of PSD on the overestimation of ITZ thickness needs to be discussed. Five kinds of PSD functions are chosen as given in the literature [32], i.e., Fuller 0.125-10, Fuller 0.25-10, Fuller 0.50-10, Fuller 0.25-20 and Fuller 0.25-40 as shown in Fig. 10(d). It can be found from the oblate κ = 0.229 ellipsoidal aggregate system that the three curves of $t_N^{\perp\prime}/t$ with D_{eq_min} = 0.25 seem to overlap. The reason is that these three aggregate systems possess similar statistical average specific surface area S_V [32], Eq.(12).

This is a preprint of a paper published in Powder Technology. The version of record can be found at https://doi.org/10.1016/j.powtec.2017.12.008

$$S_V = \int_{D_{eq\_min}}^{D_{eq\_max}} \frac{6}{sD_{eq}} f_N(D_{eq}) dD_{eq} \tag{12}$$

where s is the sphericity of particle.

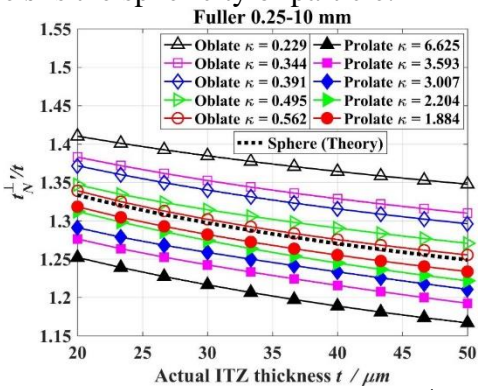

(a) Effect of spheroidal particle shape on $t_N^{\perp\prime}$ using the NLS algorithm

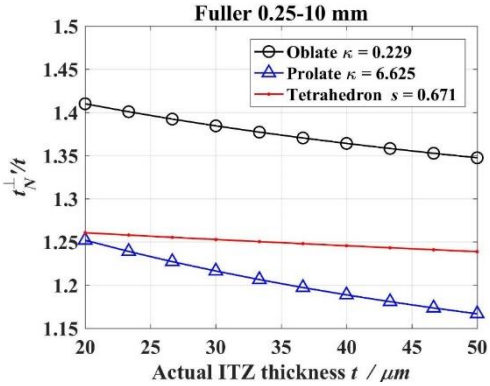

(b) Three types of particle shapes with the same sphericity, s = 0.671

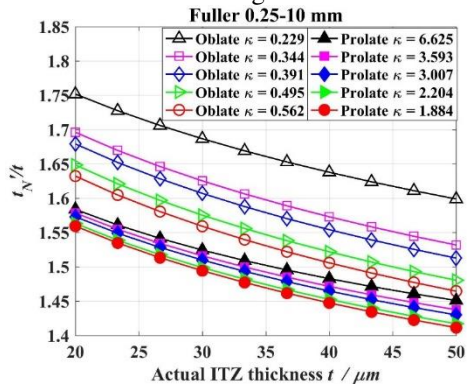

(c) Effect of spheroidal particle shape on t_N' using the SLS algorithm [40]

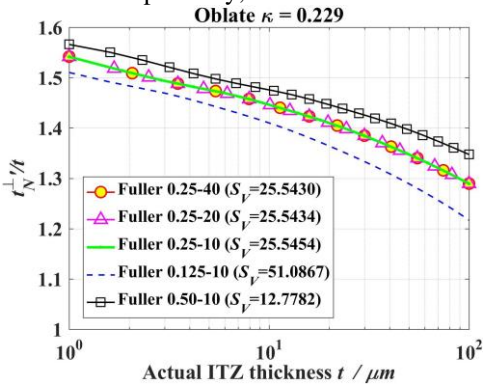

(d) Effect of PSD for oblate ellipsoids with κ = 0.229 (sphericity s = 0.671)

Fig. 10. Influences of particle shape and PSD on $t_N^{\perp\prime}/t$

Moreover, the value S_V as shown in the legend of Fig. 10(d) increases with increasing fineness of the aggregate, and the degree of overestimation of $t_N^{\perp\prime}/t$ reduces with an increase in both the actual ITZ thickness and fineness of the aggregate.

5. ITZ volume fraction overestimation

Using the values of $t_N^{\perp\prime}$ obtained from the NLS algorithm, it is possible to exactly assess the degree of overestimation of the ITZ volume fraction induced by the sectional analysis, as it is important to assess both the thickness and the volume fraction of the ITZ when predicting the transport properties of concretes. The actual ITZ volume fraction ϕ_{ITZ} and the calculated ITZ volume fraction $\phi_{ITZ}^{\perp\prime}$ can be respectively determined from t (actual ITZ thickness) and $t_N^{\perp\prime}$ according to a modified Garboczi-Bentz formula [5, 32] (denoted as the 'Chen model'), Eq.(13).

$$\phi_{ITZ} = 1 - \phi_{agg} - e_V(t) \tag{13}$$

where ϕ_{agg} and $e_V(t)$ are the volume fractions of aggregate, and of the cement paste matrix outside all aggregates and ITZs in the concrete, respectively.

This is a preprint of a paper published in Powder Technology. The version of record can be found at https://doi.org/10.1016/j.powtec.2017.12.008

$$e_V(t)=(1-\phi_{agg})\exp\left\{-2\phi_{agg}S\left[a_0\left(\frac{t}{\overline{D_{eq}}}\right)^3+a_1\left(\frac{t}{\overline{D_{eq}}}\right)^2+a_2\left(\frac{t}{\overline{D_{eq}}}\right)\right]\right\} \tag{14}$$

in which

$$\begin{aligned} a_0 &= \left[4B(1-\phi_{agg})(1-\phi_{agg}+3\phi_{agg}S)+4A\phi_{agg}^2S^2\right]/(1-\phi_{agg})^3 \\ a_1 &= \left[6B(1-\phi_{agg})+9\phi_{agg}S\right]/(1-\phi_{agg})^2 \\ a_2 &= 3/(1-\phi_{agg}) \end{aligned} \tag{15}$$

where $B=s\cdot\left(\overline{D_{eq}}\right)^2/\overline{D_{eq}^2}$, $S=\left(\overline{D_{eq}^2}\cdot\overline{D_{eq}}\right)/\left(s\cdot\overline{D_{eq}^3}\right)$, and s is the sphericity of particle, A is a constant depending on the theoretical approximation in the nearest-surface distribution functions [46-49]; values of A = 0, 2 and 3 correspond to the Percus-Yevick approximation, Carnahan-Starling approximation and Scaled-Particle approximation, respectively, and A = 0 is considered to be always the best choice to use for spherical aggregates [5]. $\overline{D_{eq}^n}$ is the n^{th}-order central moment as expressed in Eq.(16).

$$\overline{D_{eq}^n}=\int_{D_{eq\_\min}}^{D_{eq\_\max}}D_{eq}^n f_N(D_{eq})\,dD_{eq} \tag{16}$$

Recently, Xu et al. [41, 50, 51] reported the ITZ volume fraction around polydisperse ellipsoidal particles, denoted the 'Xu model'. The actual ITZ volume fraction can be obtained according to these two models, and the results are shown in Fig. 11. It is noted that there is almost no difference between two models. Thus, Chen model is chosen in this paper to calculate the ITZ volume fraction.

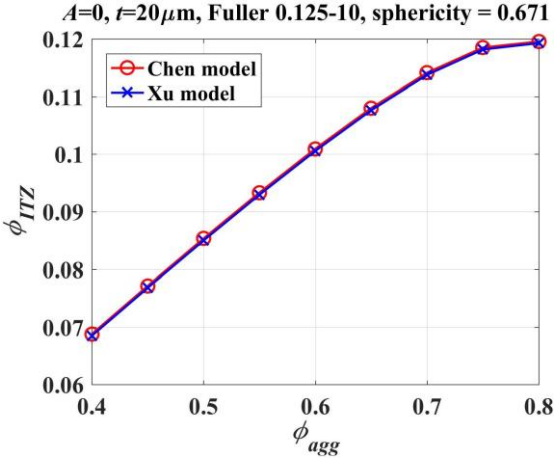

Fig. 11. Comparison of the actual ITZ volume fraction between the Chen model and the Xu model

In this section, the influences of the particle shape, PSD and sampling method on the values of $\phi_{ITZ}^{\perp\prime}/\phi_{ITZ}$ are discussed. It can be seen from Fig. 12(a) that the degree of overestimation of ITZ volume fraction decreases with increasing aggregate volume fraction under the conditions: A = 0, t = 20 μm and Fuller 0.125-10. As was the case for the thickness, the values of $\phi_{ITZ}^{\perp\prime}/\phi_{ITZ}$ decrease with increasing sphericity for oblate ellipsoidal particles when $\phi_{agg} \le 0.76$, but increase for prolate ellipsoidal particles.

Taking three types of particle shapes with the same sphericity s = 0.671 as an example, i.e., oblate κ = 0.229, prolate κ = 6.625 and tetrahedron. Fig. 12(b) shows that the order of the degree

This is a preprint of a paper published in Powder Technology. The version of record can be found at https://doi.org/10.1016/j.powtec.2017.12.008

of overestimation of $\phi_{ITZ}^{\perp\prime}/\phi_{ITZ}$ is again: oblate ellipsoid > tetrahedron > prolate ellipsoid. Fig. 12(c) also shows the difference between two sampling methods, in that the degree of overestimation of the ITZ volume fraction in the NLS algorithm is less than that in the SLS algorithm for both oblate and prolate ellipsoids.

Three PSD functions (i.e., Fuller 0.125-10, Fuller 0.25-10 and Fuller 0.50-10 mm) are selected to investigate the influence of PSD on the overestimation of ITZ volume fraction for oblate and prolate ellipsoids with the same sphericity. Fig. 12(d) shows that the values of $\phi_{ITZ}^{\perp\prime}/\phi_{ITZ}$ reduce with increasing aggregate fineness and aggregate volume fraction for both oblate and prolate ellipsoids. In addition, the degree of overestimation of the ITZ volume fraction for oblate ellipsoids is larger than that for prolate ellipsoids for a specified PSD function.

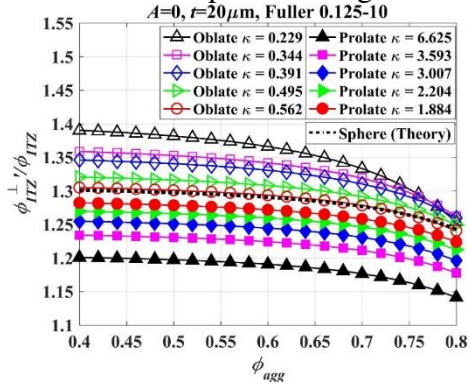

(a) Effect of spheroidal particle shape by using the NLS algorithm

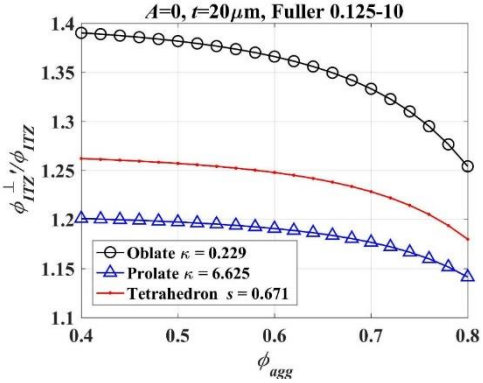

(b) Three types of particle shapes with the same sphericity, s = 0.671

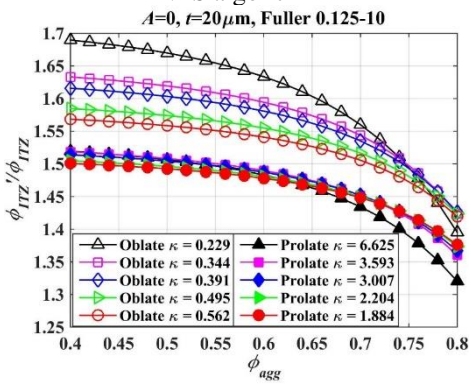

(c) Effect of spheroidal particle shape, ϕ_{ITZ}' is the ITZ volume fraction which is determined by the SLS algorithm [40]

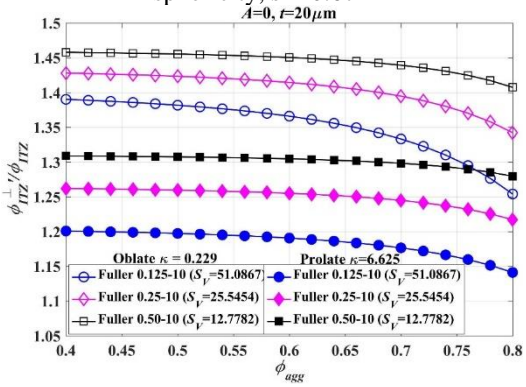

(d) Effect of PSD for spheroidal ellipsoids, sphericity s = 0.671

Fig. 12. Effects of particle shape and PSD on the overestimation of ITZ volume fraction

6. Diffusivity overestimation

A variety of theoretical models have been employed to investigate the influence of the ITZ on the macroscopic properties of cementitious composites, such as differential effective medium (DEM) method [46, 52, 53]. In the DEM approximation, the inclusions are discontinuous, and the matrix is considered to be continuous. This represents the general situation for concrete, which has discontinuous aggregates surrounded by ITZ regions, embedded in a continuous paste matrix [54-56]. The DEM analytical approximation as given in Eq.(17) is widely used [53, 57, 58], and reveals good agreement with experimental results

This is a preprint of a paper published in Powder Technology. The version of record can be found at https://doi.org/10.1016/j.powtec.2017.12.008

[53, 59], so is adopted in this paper to calculate the diffusivity of a mobile species within the composite.

$$\left(\frac{D_{cp}}{D_{con}}\right)^{1/3}\left(\frac{D_{con}-D_e}{D_{cp}-D_e}\right)=1-\phi_{agg}-\phi_{ITZ} \tag{17}$$

where D_{con}, D_{cp} and D_{ITZ} are the diffusivities within concrete, cement paste matrix and the ITZ, respectively, $D_e=2\phi_{ITZ}D_{ITZ}/(3\phi_{agg}+2\phi_{ITZ})$, and ϕ_{agg} and ϕ_{ITZ} are the volume fractions of aggregate and ITZ, respectively.

The diffusivity within the concrete, as calculated from the actual ITZ thickness t and the statistical average of the apparent ITZ thickness $t_N^{\perp\prime}$, are expressed as D_{con} and $D_{con}^{\perp\prime}$, respectively. In this section, the influences of the D_{ITZ}/D_{cp}, particle shape, PSD and sampling method on the degree of overestimation of the diffusivity is analysed. Normally, the diffusivity of the ITZ is taken as an integer multiple of the diffusivity of cement paste. For instance, ratios D_{ITZ}/D_{cp} = 3, 5 or 7, for oblate spheroids at κ = 0.229, are used here to evaluate the degree of overestimation of the diffusivity under the conditions of A = 0, actual ITZ thickness t = 20 μm, Fuller 0.125-10 mm grading. The results are shown in Fig. 13 ; the overestimation of diffusivity increases with increasing D_{ITZ}/D_{cp} at a given aggregate volume fraction.

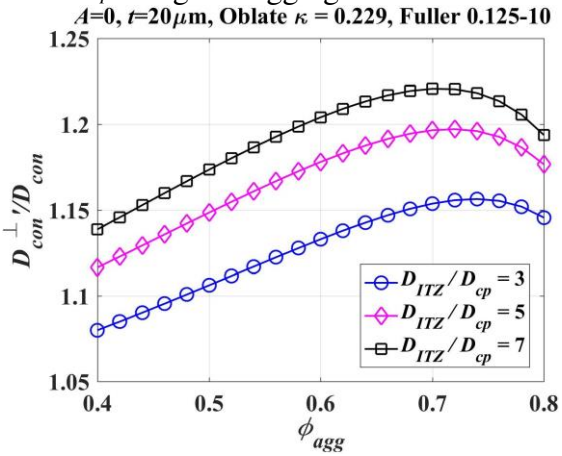

Fig. 13. Effect of D_{ITZ}/D_{cp} on the overestimation of diffusivity within concrete

Taking D_{ITZ}/D_{cp} = 5 [32] as an example, the results are shown in Fig. 14 under the conditions: A = 0, t = 20 μm, Fuller 0.125-10 mm. Fig. 14(a) shows that the values of $D_{con}^{\perp\prime}/D_{con}$ increase at first, but subsequently drop down, with an increase in aggregate volume fraction. The values of $D_{con}^{\perp\prime}/D_{con}$ decrease with increasing sphericity for oblate ellipsoids, but increase for prolate ellipsoids. Compared with the spherical particle (sphericity s = 1), the order of the degree of overestimation of concrete diffusivity is: oblate ellipsoid > sphere > prolate ellipsoid. However, taking three types of particle shapes with the same sphericity s = 0.671 as an example, i.e., oblate κ = 0.229, prolate κ = 6.625 and tetrahedron, Fig. 14(b) shows that the order of the degree of overestimation of $D_{con}^{\perp\prime}/D_{con}$ is: oblate ellipsoid > tetrahedron > prolate ellipsoid. Fig. 14(c) shows the difference between the two sampling methods; the degree of overestimation of the diffusivity calculated using the NLS algorithm is less than that in the SLS algorithm for both oblate and prolate ellipsoids.

This is a preprint of a paper published in Powder Technology. The version of record can be found at https://doi.org/10.1016/j.powtec.2017.12.008

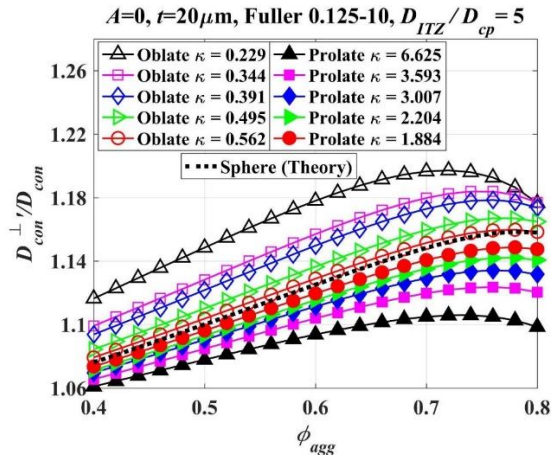

(a) Effect of spheroidal particle shape by using the NLS algorithm

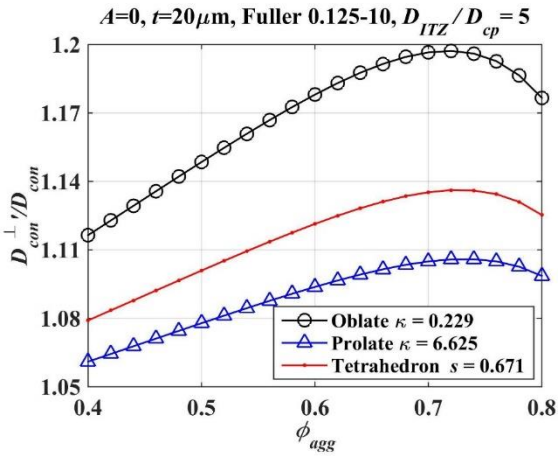

(b) Three types of particle shapes with the same sphericity, s = 0.671

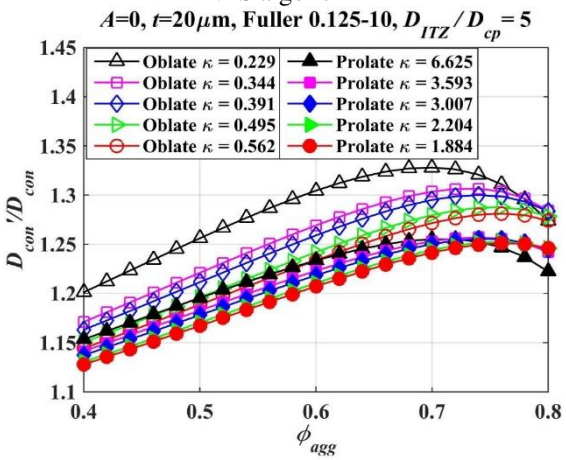

(c) Effect of spheroidal particle shape, D_{con}' is the diffusivity determined by the SLS algorithm [40]

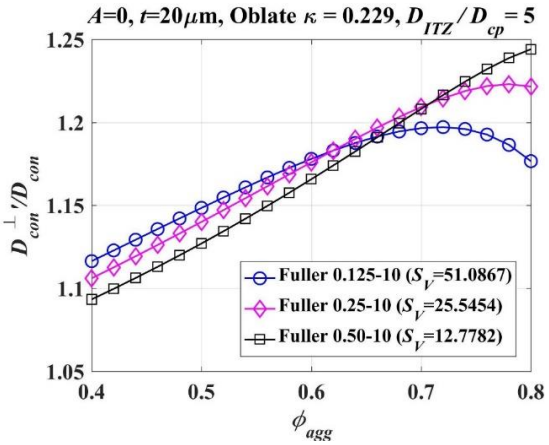

(d) Effect of PSD for oblate κ = 0.229 (sphericity s = 0.671)

Fig. 14. Effects of particle shape and PSD on the overestimation of diffusivity within concrete

Lastly, taking oblate ellipsoids with κ =0.229 as an example, three PSD functions (Fuller 0.125-10, Fuller 0.25-10 and Fuller 0.50-10 mm), we consider the effect of PSD on the values of $D_{con}^{\perp}{}'/D_{con}$, as shown in Fig. 14(d). This calculation indicates that the degree of overestimation of $D_{con}^{\perp}{}'/D_{con}$ increases with increasing aggregate fineness when ϕ_{agg} is in the range 0.40 – 0.60. Conversely, the values of $D_{con}^{\perp}{}'/D_{con}$ reduce with increasing aggregate fineness when ϕ_{agg} > 0.72.

7. Conclusions

An interfacial transition zone (ITZ) layer model around an ellipsoidal particle, along with the normal line sampling (NLS) algorithm, have been employed in this paper to investigate the influence of the particle shape on the overestimation of the ITZ thickness by statistical sampling methods. A line sampling rule with $N_\theta = N_\phi$ = 20, $\Delta L_{3D} = \Delta L_{2D} = 0.005 D_{eq}$ was determined to be appropriate for application of the NLS algorithm to spheroidal particles. The ratio of the apparent to the actual ITZ thickness $t_\perp' / t$ is used to characterize the degree of overestimation

of the ITZ thickness; this is significantly influenced by the particle shape. The values of $t_{\perp}'/t$ decrease with increasing sphericity for oblate ellipsoidal particles, but increase for prolate ellipsoidal particles. Compared with a spherical particle (sphericity s = 1), the degree of overestimation of the ITZ thickness is: oblate ellipsoid > sphere > prolate ellipsoid, and increasing with decreased sphericity for each of the types of ellipsoid. The degree of overestimation of the ITZ thickness for oblate ellipsoids is up to 9.3% greater than for spherical particles, but lower by as much as up to 6.6% for prolate ellipsoids than for spherical particles. However, no clear trend exists between Platonic and spheroidal particles of the same sphericity. The NLS algorithm resembles the experimental process for determining the ITZ thickness, and yields a lower degree of ITZ thickness overestimation than does the systematic line sampling (SLS) algorithm for spheroidal ellipsoids. For a polydisperse aggregate system, the value of $t_N^{\perp}{}'/t$ is governed by the sphericity of the particles, the particle size distribution of the aggregate, and the actual ITZ thickness. Finally, the degree of overestimation of ITZ volume fraction $\phi_{ITZ}^{\perp}{}'/\phi_{ITZ}$ and of diffusivity within concrete $D_{con}^{\perp}{}'/D_{con}$ resulting from the sampling of the ITZ are evaluated. The results indicate that the values of $\phi_{ITZ}^{\perp}{}'/\phi_{ITZ}$ reduce when increasing both aggregate volume fraction and fineness of aggregate. The degree of overestimation of diffusivity is governed by aggregate volume fraction, fineness of aggregate and particle shape.

This work highlights that aggregate shape has a significant effect on the apparent ITZ thickness, ITZ volume fraction, and further on the macroscopic transport properties of cementitious composites. Dehghanpoor Abyaneh et al. [60] also pointed out that the shape and orientation of aggregate particles have a significant effect on diffusivity ; such effects remain to be captured by models of the type presented here. The sphericity of a particle is an important parameter to quantitatively generalize the effect of particle shape, but it is not a unique one, nor is it sufficient to fully define the governing relationship. It is therefore important to consider particle shape parameters that will enable us to obtain an analytical formula for the influence of particle shape on the degree of overestimation of the ITZ thickness in the future.

Acknowledgements

Z.G. Zhu and H.S. Chen gratefully acknowledge the financial support from the National Nature Science Foundation of China via Grant No. 51461135001, the Ministry of Science and Technology of China ‘‘973 Project” via Grant No. 2015CB655102, and the Fundamental Research Funds for the Central Universities via Grant No. 2242016K41054. Z.G. Zhu also gratefully appreciates the Scientific Research Foundation of Graduate School of Southeast University via Grant No. YBJJ1452. The contributions of J.L. Provis have been supported by the Engineering and Physical Sciences Research Council (UK) under grant EP/M003272/1.

Appendix A. Supplementary data for the NLS algorithm

Taking two spheroidal particles with the same sphericity (i.e., oblate ellipsoid with κ = 0.229 and prolate ellipsoid with κ = 6.625) as an example, the total number of sampling lines is about 10^5, 10^6, 10^7 and 10^8 when $N\theta$ is 3, 5, 10 and 20, respectively. Both probability density curves and cumulative probability curves of $t_{\perp}'/t$ are shown in Figure A-1(a), which reveals that the

This is a preprint of a paper published in Powder Technology. The version of record can be found at https://doi.org/10.1016/j.powtec.2017.12.008

curves become smoother with an increase of the total number of sampling lines. When the total number of sampling lines reaches 10^8, the curves of probability density and cumulative probability are smooth enough to represent their actual distribution. So, a total number of sampling lines of 10^8 is further used to study the influence of particle shape on the probability distribution curves of $t_\perp'/t$. Figure A-1(b) shows that if the total number of sampling lines reaches 10^8, no significant difference in the overall curves of $t_\perp'/t$ occurs among oblate and prolate ellipsoids with different sphericities as given in Table 1. However, a slight discrepancy can still be found in the zoomed-in inset region at smaller values of $t_\perp'/t$. Therefore, the line sampling rule of the NLS algorithm ($N_\theta = N_\phi$ = 20, $\Delta L_{3D} = \Delta L_{2D} = 0.005 D_{eq}$) is acceptable, and is employed in this study.

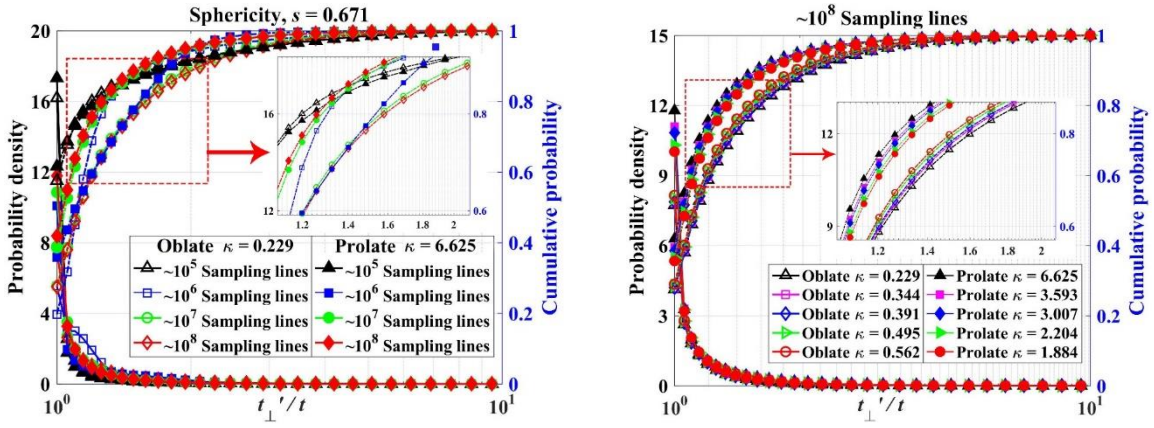

(a) Statistical distribution of $t_\perp'/t$ for spheroidal particle at different total numbers of sampling lines

(b) Oblate and prolate ellipsoidal particles at 10^8 sampling lines

Figure A-1. Probability density and cumulative probability distributions of $t_\perp'/t$

Appendix B. Comparison of effect of particle shapes on $t_\perp'/t$

The relative degrees of error between non-spherical and spherical particles in terms of the degree of overestimation of the ITZ thickness can be calculated from Fig. 8(a) according to Eq.(18).

$$\text{Relative error of } t_\perp'/t = \frac{(t_\perp'/t)_{object} - (t_\perp'/t)_{sphere}}{(t_\perp'/t)_{sphere}} \times 100\% \tag{18}$$

where *object* = oblate ellipsoid, prolate ellipsoid, and five kinds of Platonic particles, respectively.

Relative errors in $t_\perp'/t$ between spheroidal and spherical particles increase with decreasing sphericity, as shown in Figure B-1(a). The ITZ thickness for oblate ellipsoids is overestimated by up to 9.3% more than for spherical particles, while the estimation degree of the ITZ thickness for prolate ellipsoids is overestimated by up to 6.6% less. Similarly, the relative errors of $t_\perp'/t$ between Platonic [34] and spherical particles are shown in Figure B-

1(b). The relative errors of $t_{\perp}'/t$ increase with decreasing sphericity, and the ITZ thickness for Platonic particles may be overestimated by up to 5.4% more or by up to 16.8% less than for spherical particles, depending on t/D_{eq}.

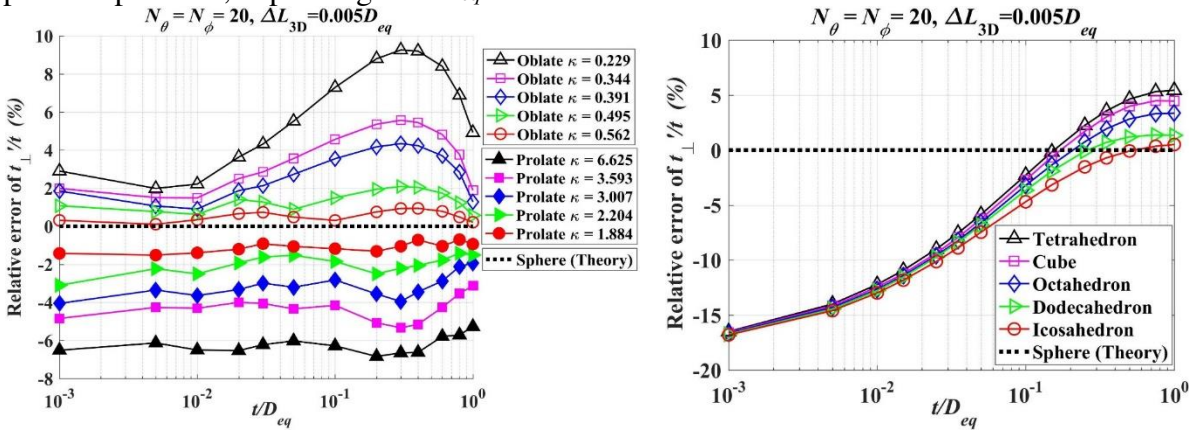

(a) Oblate and prolate ellipsoids (b) Platonic particles

Figure B-1. Relative error of the overestimation of the ITZ thickness based on the NLS algorithm

References

[1] K.L. Scrivener, A.K. Crumbie, P.L. Pratt, A study of the interfacial region between cement paste and aggregate in concrete, in: S.P. Shah, S. Mindess (Eds.) Bonding in Cementitious Composites, MRS Proceedings, vol. 114, Materials Research Society, Pittsburgh, 1988, pp. 87-88.

[2] O.P. Kari, Y. Elakneswaran, T. Nawa, J. Puttonen, A model for a long-term diffusion of multispecies in concrete based on ion–cement-hydrate interaction, J. Mater. Sci., 48 (2013) 4243-4259.

[3] K.L. Scrivener, K.M. Nemati, The percolation of pore space in the cement paste/aggregate interfacial zone of concrete, Cem. Concr. Res., 26 (1996) 35-40.

[4] H.S. Chen, W. Sun, P. Stroeven, Interfacial transition zone between aggregate and paste in cementitious composites (II): Mechanism of formation and degradation of interfacial transition zone microstructure and its influence factors, J. Chin. Ceram. Soc. (in Chinese), 32 (2004) 70-79.

[5] E.J. Garboczi, D.P. Bentz, Analytical formulas for interfacial transition zone properties, Adv. Cem. Based Mater., 6 (1997) 99-108.

[6] W.X. Xu, H.S. Chen, W. Chen, L.H. Jiang, Prediction of transport behaviors of particulate composites considering microstructures of soft interfacial layers around ellipsoidal aggregate particles, Soft Matter, 10 (2014) 627-638.

[7] H.Y. Ma, D.S. Hou, Z.J. Li, Two-scale modeling of transport properties of cement paste: Formation factor, electrical conductivity and chloride diffusivity, Comput. Mater. Sci., 110 (2015) 270-280.

[8] M.K. Head, H.S. Wong, N.R. Buenfeld, Characterising aggregate surface geometry in thin-sections of mortar and concrete, Cem. Concr. Res., 38 (2008) 1227-1231.

[9] P.K. Dehdezi, S. Erdem, M.A. Blankson, Physico-mechanical, microstructural and dynamic properties of newly developed artificial fly ash based lightweight aggregate - rubber concrete composite, Compos. Part B-Eng., 79 (2015) 451-455.

[10] Q. Wang, P.Y. Yan, J.W. Yang, B. Zhang, Influence of steel slag on mechanical properties and durability of concrete, Constr. Build. Mater., 47 (2013) 1414-1420.
[11] P.G. Allison, C.A. Weiss jr., R.D. Moser, A.J. Diaz, O.G. Rivera, S.S. Holton, Nanoindentation and SEM/EDX characterization of the geopolymer-to-steel interfacial transition zone for a reactive porcelain enamel coating, Compos. Part B-Eng., 78 (2015) 131-137.
[12] H.S. Wong, M. Zobel, N.R. Buenfeld, R.W. Zimmerman, Influence of the interfacial transition zone and microcracking on the diffusivity, permeability and sorptivity of cement-based materials after drying, Mag. Concr. Res., 61 (2009) 571-589.
[13] F.H. Han, Q. Wang, J.J. Feng, The differences among the roles of ground fly ash in the paste, mortar and concrete, Constr. Build. Mater., 93 (2015) 172-179.
[14] E.W. Tiedje, P.J. Guo, Modeling the influence of particulate geometry on the thermal conductivity of composites, J. Mater. Sci., 49 (2014) 5586-5597.
[15] L.Y. Li, D. Easterbrook, J. Xia, W.L. Jin, Numerical simulation of chloride penetration in concrete in rapid chloride migration tests, Cem. Concr. Compos., 63 (2015) 113-121.
[16] W.X. Xu, H.F. Ma, S.Y. Ji, H.S. Chen, Analytical effective elastic properties of particulate composites with soft interfaces around anisotropic particles, Composites Science and Technology, 129 (2016) 10-18.
[17] Y. Jiao, S. Torquato, Quantitative characterization of the microstructure and transport properties of biopolymer networks, Phys. Biol., 9 (2012) 036009.
[18] W.X. Xu, H.S. Chen, W. Chen, Z.G. Zhu, Theoretical estimation for the volume fraction of interfacial layers around convex particles in multiphase materials, Powder Technol., 249 (2013) 513-515.
[19] W.X. Xu, H.S. Chen, Analytical and modeling investigations of volume fraction of interfacial layers around ellipsoidal aggregate particles in multiphase materials, Modelling Simul. Mater. Sci. Eng., 21 (2013) 015005.
[20] W.X. Xu, H. Wang, Y.Z. Niu, J.T. Bai, Insight into interfacial effect on effective physical properties of fibrous materials. I. The volume fraction of soft interfaces around anisotropic fibers, J. Chem. Phys., 144 (2016) 014703.
[21] K. Wu, H.S. Shi, L.L. Xu, G. Ye, G. De Schutter, Microstructural characterization of ITZ in blended cement concretes and its relation to transport properties, Cem. Concr. Res., 79 (2016) 243-256.
[22] X.M. Song, F.L. Meng, M.G. Kong, Y.Z. Wang, L.P. Huang, X.B. Zheng, Y. Zeng, Thickness and microstructure characterization of TGO in thermal barrier coatings by 3D reconstruction, Mater. Charact., 120 (2016) 244-248.
[23] K.L. Scrivener, Backscattered electron imaging of cementitious microstructures: understanding and quantification, Cem. Concr. Compos., 26 (2004) 935-945.
[24] Y. Gao, G. De Schutter, G. Ye, Z.J. Tan, K. Wu, The ITZ microstructure, thickness and porosity in blended cementitious composite: Effects of curing age, water to binder ratio and aggregate content, Compos. Part B-Eng., 60 (2014) 1-13.
[25] K.L. Scrivener, A.K. Crumbie, P. Laugesen, The interfacial transition zone (ITZ) between cement paste and aggregate in concrete, Interface Science, 12 (2004) 411-421.
[26] P. Stroeven, Analytical and computer-simulation approaches to the extent of the interfacial transition zone in concrete, in: A.M. Brandt, V.C. Li, I.H. Marshall (Eds.) Proceedings of the Sixth International Symposium on Brittle Matrix Composites, Woodhead, Warsaw, 2000, pp. 465-474.
[27] H.S. Chen, W. Sun, Q.X. Zhao, P. Stroeven, Overestimation of thickness of interface transition zone of aggregate in concrete by sectional analysis method, J. Chin. Ceram. Soc. (in Chinese), 31 (2003) 1130-1134.
[28] Z.G. Zhu, H.S. Chen, Overestimation of ITZ thickness around regular polygon and ellipse aggregate, Comput. Struct., 182 (2017) 205-218.
[29] H.S. Chen, W. Sun, P. Stroeven, L.J. Sluys, Overestimation of the interface thickness around convex-shaped grain by sectional analysis, Acta Mater., 55 (2007) 3943-3949.

[30] J. Serra, Image Analysis and Mathematical Morphology. Vol. 2: Theoretical Advances, Academic Press, London, 1988.
[31] W.X. Xu, H.S. Chen, Q.L. Duan, W. Chen, Strategy for interfacial overlapping degree in multiphase materials with complex convex particles, Powder Technol., 283 (2015) 455-461.
[32] H.S. Chen, Z.G. Zhu, L. Liu, W. Sun, C.W. Miao, Aggregate shape effect on the overestimation of ITZ thickness: quantitative analysis of Platonic particles, Powder Technol., 289 (2016) 1-17.
[33] S. Torquato, Y. Jiao, Dense packings of the Platonic and Archimedean solids, Nature, 460 (2009) 876-879.
[34] Z.G. Zhu, H.S. Chen, L. Liu, X.Y. Li, Multi-scale modelling for diffusivity based on practical estimation of interfacial properties in cementitious materials, Powder Technol., 307 (2017) 109-118.
[35] R. San Nicolas, J.L. Provis, The interfacial transition zone in alkali-activated slag mortars, Front. Mater., 2 (2015) 70.
[36] Z.G. Zhu, H.S. Chen, W.X. Xu, L. Liu, Parking simulation of three-dimensional multi-sized star-shaped particles, Modelling Simul. Mater. Sci. Eng., 22 (2014) 035008.
[37] Z.W. Qian, E.J. Garboczi, G. Ye, E. Schlangen, Anm: a geometrical model for the composite structure of mortar and concrete using real-shape particles, Mater. Struct., 49 (2016) 149-158.
[38] E.J. Garboczi, J.W. Bullard, 3D analytical mathematical models of random star-shape particles via a combination of X-ray computed microtomography and spherical harmonic analysis, Adv. Powder Technol., 28 (2017) 325-339.
[39] Z.Y. Zhou, R.P. Zou, D. Pinson, A.B. Yu, Dynamic simulation of the packing of ellipsoidal particles, Ind. Eng. Chem. Res., 50 (2011) 9787-9798.
[40] W.R. Wang, H.S. Chen, X.Y. Li, Z.G. Zhu, Corrosion behavior of steel bars immersed in simulated pore solutions of alkali-activated slag mortar, Constr. Build. Mater., 143 (2017) 289-297.
[41] W.X. Xu, Q.L. Duan, H.F. Ma, W. Chen, H.S. Chen, Interfacial effect on physical properties of composite media: Interfacial volume fraction with non-spherical hard-core-soft-shell-structured particles, Sci. Rep., 5:16003 (2015).
[42] J.E. Hilliard, The calculation of the mean caliper diameter of a body for use in the analysis of the number of particles per unit volume, in: H. Elias (Ed.) Proceedings of the Second International Congress for Stereology, Springer, Chicago, 1967, pp. 211-215.
[43] L.M.C. Orive, Particle size-shape distributions: the general spheroid problem, J. Microsc., 107 (1976) 235-253.
[44] W.X. Xu, W. Chen, H.S. Chen, Modeling of soft interfacial volume fraction in composite materials with complex convex particles, J. Chem. Phys., 140 (2014) 034704.
[45] L. Liu, D.J. Shen, H.S. Chen, W.X. Xu, Aggregate shape effect on the diffusivity of mortar: a 3D numerical investigation by random packing models of ellipsoidal particles and of convex polyhedral particles, Comput. Struct., 144 (2014) 40-51.
[46] S. Torquato, Random Heterogeneous Materials: Microstructure and Macroscopic Properties, Springer, New York, 2005.
[47] B.L. Lu, S. Torquato, Nearest-surface distribution functions for polydispersed particle systems, Phys. Rev. A, 45 (1992) 5530-5544.
[48] S. Torquato, B. Lu, J. Rubinstein, Nearest-neighbor distribution functions in many-body systems, Phys. Rev. A, 41 (1990) 2059-2075.
[49] S. Torquato, Effect of dimensionality on the continuum percolation of overlapping hyperspheres and hypercubes, J. Chem. Phys., 136 (2012) 054106.
[50] W.X. Xu, F. Wu, Y. Jiao, M.J. Liu, A general micromechanical framework of effective moduli for the design of nonspherical nano- and micro-particle reinforced composites with interface properties, Mater. Des., 127 (2017) 162-172.
[51] W. Xu, B. Xu, F. Guo, Elastic properties of particle-reinforced composites containing nonspherical particles of high packing density and interphase: DEM–FEM simulation and micromechanical theory, Comput. Method Appl. M., 326 (2017) 122-143.

[52] V.D. Bruggeman, Berechnung verschiedener physikalischer konstanten von heterogenen substanzen. I. Dielektrizitätskonstanten und leitfähigkeiten der mischkörper aus isotropen substanzen, Annalen der Physik, 416 (1935) 636-664.
[53] J.J. Zheng, X.Z. Zhou, H.Y. Xing, X.Y. Jin, Differential effective medium theory for the chloride diffusivity of concrete, ACI Mater. J., 111 (2014) 1-6.
[54] L. Liu, W. Sun, G. Ye, H.S. Chen, Z.W. Qian, Estimation of the ionic diffusivity of virtual cement paste by random walk algorithm, Constr. Build. Mater., 28 (2012) 405-413.
[55] L. Liu, H.S. Chen, W. Sun, G. Ye, Microstructure-based modeling of the diffusivity of cement paste with micro-cracks, Constr. Build. Mater., 38 (2013) 1107-1116.
[56] F. Montero-Chacón, J. Marín-Montín, F. Medina, Mesomechanical characterization of porosity in cementitious composites by means of a voxel-based finite element model, Comput. Mater. Sci., 90 (2014) 157-170.
[57] E.J. Garboczi, J.G. Berryman, Elastic moduli of a material containing composite inclusions: effective medium theory and finite element computations, Mech. Mater., 33 (2001) 455-470.
[58] L. Gao, X.F. Zhou, Differential effective medium theory for thermal conductivity in nanofluids, Phys. Lett. A, 348 (2006) 355-360.
[59] C.C. Yang, J.K. Su, Approximate migration coefficient of interfacial transition zone and the effect of aggregate content on the migration coefficient of mortar, Cem. Concr. Res., 32 (2002) 1559-1565.
[60] S. Dehghanpoor Abyaneh, H.S. Wong, N.R. Buenfeld, Modelling the diffusivity of mortar and concrete using a three-dimensional mesostructure with several aggregate shapes, Comput. Mater. Sci., 78 (2013) 63-73.